 doi:10.20944/preprints202208.0296.v1

Savonius Wind Turbine Performance Comparison with One and Two Porous Deflectors: A CFD Study

Md Mahmud Hasan Saikot[a,*], Mahfuzur Rahman[a], Md Anwar Hosen[b], Wasif Ajwad[a], Md. Faiyaz Jamil[c], Md Quamrul Islam[a]

[a]*Department of Mechanical Engineering, Bangladesh University of Engineering and Technology, Dhaka 1000, Bangladesh.*
[b]*Department of Mechanical Engineering, Pennsylvania State University, University Park, PA 16802, United States.*
[c]*Department of Mechanical Engineering, University of Massachusetts Dartmouth, North Dartmouth, MA 02747, United States.*

[*]*Corresponding author email: saikath65@gmail.com*

Abstract

The present study explores the effect of using two porous deflectors on the performance of the Savonius wind turbine compared to only one porous deflector. The numerical simulation is performed to solve the unsteady Navier-Stokes equations using the SST k-ω turbulence model. The porous deflectors under consideration are placed upstream of a Savonius wind turbine. To improve turbine performance, deflector parameters such as porosity, angle, position, and length are varied for one of the deflectors placed near the advancing blade. The second deflector in front of the returning blade is retained in a previously optimized configuration. Then the finalized configuration with two porous deflectors is compared to the previous single porous deflector configuration. At a tip speed ratio of 0.9, the finalized two porous deflector configuration exhibits a 26% higher power coefficient than the single porous deflector case and delivers positive torque throughout the cycle. The maximum variation of torque coefficient in a cycle is found to be 6% lower as well. Due to the increased blockage effect for two deflectors, suitable domain dimensions are also studied to mitigate the overestimation of the performance coefficient. The self-starting capability of the turbine is improved significantly for the azimuthal angle of 80° as well.

Keywords: Savonius wind turbine; Porous deflector; Porosity; Computational Fluid Dynamics (CFD); Self-starting

Preprints (www.preprints.org) | NOT PEER-REVIEWED | Posted: 17 August 2022 doi:10.20944/preprints202208.0296.v1

Nomenclature

θ	Azimuthal angle [°]
β	Angle of the upper porous deflector [°]
ω	Angular velocity of the turbine [rad/s]
A	Area swept by the turbine [m^2]
ρ	Density of air [kg/m^3]
D	Diameter of the turbine [m]
d	Diameter of the bucket [m]
D_r	Diameter of the rotating domain [m]
μ	Dynamic viscosity of the fluid [kg/ms]
L_1	Horizontal distance of the inlet measured from the center of the turbine [m]
L_2	Horizontal distance of the outlet measured from the center of the turbine [m]
X	Horizontal distance of the porous upper deflector from the center of the turbine [m]
U_∞	Inlet velocity of the fluid [m/s]
C_2	Inertial Resistance [1/m]
L	Length of the porous upper deflector [m]
C_m	Instantaneous moment coefficient [-]
$C_{m,avg}$	Average moment coefficient [-]
e	Overlap length [m]
K	Permeability [m^2]
P_t	Power [W]
C_p	Instantaneous power coefficient [-]
$C_{p,avg}$	Average power coefficient [-]
ψ	Porosity of the upper deflector [-]
D_L	Lower porous deflector [-]
D_U	Upper porous deflector [-]
P	Pressure [Pa]
R	Radius of the turbine [m]

Preprints (www.preprints.org) | NOT PEER-REVIEWED | Posted: 17 August 2022 doi:10.20944/preprints202208.0296.v1

C_{ms}	Static moment coefficient [-]
t	Thickness of the bucket [m]
λ	Tip Speed Ratio [-]
T	Torque [N.m]
W_1	Vertical distance of the upper symmetry wall from the center of the turbine [m]
W_2	Vertical distance of the lower symmetry wall from the center of the turbine [m]
Y	Vertical distance of the porous upper deflector from the center of the turbine [m]

1. Introduction

Global warming and the increase in greenhouse gas emissions have been the burning issue over the last few decades. The significant change in global climate has been the key driver and motivation for finding renewable energy options over fossil fuels worldwide. In particular, solar and wind resources are receiving a lot of interest because they are clean and pollution-free energies. Wind is one of the most powerful green energy sources, and it can be used to support global electricity by more than 20% by 2030 [1]. Wind energy has emerged as a viable renewable energy supply due to recent technological breakthroughs that have resulted in more efficient turbine designs. The two kinds of wind turbines used to capture wind energy are horizontal-axis wind turbines (HAWTs) and vertical-axis wind turbines (VAWTs) [2]–[4]. There are two types of VAWT: lift-type Darrieus turbines and drag-type Savonius turbines. Savonius wind turbines provide a number of advantages, including ease of construction and low cost, independence from wind direction, and an acceptable starting torque at low wind speeds [5], [6]. These distinctive characteristics have motivated many researchers to work on improving the performance of the Savonius turbine [7]. Numerous experimental and computational studies have been conducted to determine the effect of different design factors on the turbine's performance such as the number of buckets, the distance between the rotor buckets, the rotor's aspect ratio, and the overlap ratio [8]–[10]. Several studies on the modification of blade profile also have been carried out to increase the efficiency of the turbine [11]–[17]. To improve the Savonius turbine's aerodynamic performance, various power augmentation devices such as deflector plates [18], guide vanes [19], windshields[20], nozzles [21], curtain plates [22], quarter blades [23], and miniature blades [24] were introduced by researchers worldwide.

One suggestion for increasing the efficiency of the Savonius turbine was to use a V-shaped deflector placed upstream of the rotors by Shaughnessy and Probert [25], which lowered the air-flow resistance met by the portion of the wind turbine blade advancing towards the wind. They determined the optimum deflector configuration by changing the deflector's location relative to the rotor and the wedge angle between the deflector blades. They reported that the rotor harvested

 doi:10.20944/preprints202208.0296.v1

around 20% more power than a conventional Savonius rotor when the deflector was configured optimally. Stout et al. [26] suggested an upstream deflector as one of the simplest power augmentation devices for reducing the negative torque on the returning blade and redirecting the airflow from the returning blade. They reported that the addition of a deflector resulted in a substantial increase in turbine output power compared to open rotor designs. Golecha et al. [27] conducted experimental research to determine the effect of the deflector plate's position on the performance of a modified Savonius rotor. Using eight different deflector plate positions, they found that the coefficient of power improved by 50% when the deflector plate is in its optimum position. The maximum coefficient of power was determined to be 0.21 at a tip speed ratio of 0.82 in their study.

Putri et al. [28] examined the impact of an upstream obstruction on the performance of a Savonius wind turbine experimentally. The obstacle had a substantial effect on the mechanical torque and power output of the rotor, while the Reynolds number had little effect on the rotor output power. Guo et al. [29] investigated the effects of the rear deflector on the performance of the Savonius turbine using both numerical and experimental approaches. They concluded that equipping the Savonius turbine with a deflector would be a cost-effective method to increase its output power. Their findings indicated that the impact on the power coefficient decreased as the deflector's length and distance from the center of rotation increased. The optimum deflector location was found to be 0.82 times the turbine's diameter relative to the turbine's center of rotation. Mohamed et al. [30] partly shielded the returning blade with an obstruction plate. As a result, the output power coefficient improved by about 27% in comparison to a standard Savonius turbine. Kim and Gharib [31] examined the output power of two lift-based counter-rotating VAWTs with an upstream flat-plate deflector. They reported that the deflector enhanced the counter-rotating VAWTs' power output. Furthermore, the deflector's shape and its distance from the turbines had a significant effect on power production. Kailash et al. [32] analyzed the impact of two deflector plates positioned upstream of the wind flow on the output of the Savonius wind turbine. They determined the optimal position for the deflector plates and found a 35% improvement in power production. Youssef et al. [33] introduced a novel method for enhancing the performance of the Savonius wind turbine by including an upstream deflector and a downstream baffle. They concluded that optimizing the deflector and baffle design increased the power coefficient from 0.24 to 0.47 at a tip speed ratio closer to unity.

According to the abovementioned literature study, the usage of solid deflectors has gained significant attention from many researchers seeking to increase the efficiency of the Savonius wind turbine. Alternatively, porous deflectors might be used to enhance performance as well. Nimvari et al. [34] computationally studied how one porous deflector positioned upstream at the front of the returning blade could enhance the performance of a Savonius turbine. The porous deflector permitted wind to pass through it, causing the wake zone behind its deflector to collapse. Consequently, the flow patterns became more uniform and less turbulent. They reported a 10%

Preprints (www.preprints.org) | NOT PEER-REVIEWED | Posted: 17 August 2022 doi:10.20944/preprints202208.0296.v1

improvement in power coefficient at a tip speed ratio of 1 by optimizing the porous deflector design. Moreover, the static torque coefficient was doubled for a certain range of rotation angles.

The primary aim of this research is to install two porous deflectors upstream to investigate the combined impact of both porous deflectors on the performance of the Savonius wind turbine using a CFD approach. To accomplish this, one deflector was maintained at the optimum condition as suggested by Nimvari et al. [34], while the other deflector parameters were varied for maximum performance. Then, the resulting two porous deflector configuration was compared with the single porous deflector case.

2. Computational domain and grid

Following the experimental case of Sheldhal et al. [8], a 2D geometrical model of a two-bladed Savonius turbine was taken into consideration (Fig. 1). The geometrical parameters for the turbine rotor are given in Table 1. Fig. 2 depicts the computational domain, boundary conditions, and other parameters. L_1 and L_2 are the respective distance of the inlet and the outlet, measured from the center of the turbine (Fig. 2). Similarly, W_1 and W_2 are the distances of the horizontal symmetry walls from the turbine center. Two porous deflectors were placed upstream aiming to increase the power output of the turbine. The upper deflector and the lower deflector are labeled as D_U and D_L respectively. The position of the lower porous deflector (D_L) was fixed according to the optimum position of Nimvari et al. [34]. The upper deflector position, size, and other parameters such as – porosity(ψ), angle (β), length (L), horizontal distance (X), and vertical distance (Y) were varied to determine the optimum condition. Table 2 lists all the parameters for both porous deflectors.

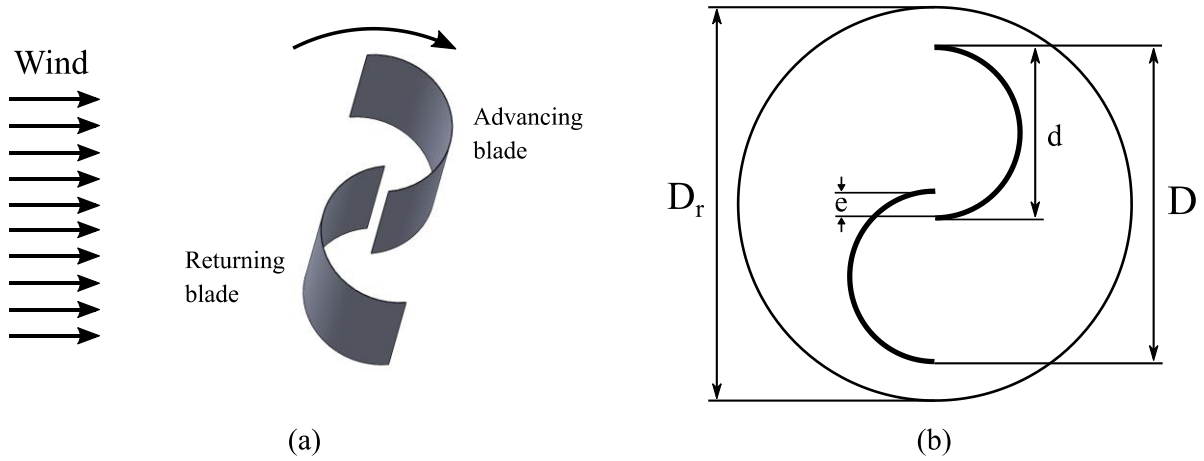

Fig. 1. (a) Savonius wind turbine blades. (b) Rotating domain and turbine dimensions.

Different zones and boundary conditions are indicated in different colors in Fig. 2. Sliding Mesh Model (SMM) was implemented with an interface assigned between the rotating and the stationary domain [35]. The density of the air was 1.25 kg/m^3 and the viscosity was 1.7894×10^{-5} kg/ms.

Preprints (www.preprints.org) | NOT PEER-REVIEWED | Posted: 17 August 2022 doi:10.20944/preprints202208.0296.v1

The inlet velocity was set to $U_\infty = 7\ m/s$. The outlet was specified to be a pressure outlet. The boundaries parallel to the flow direction were defined as symmetry walls. A no-slip wall condition was employed at the turbine blades.

Table 1. Geometrical parameters of the Savonius turbine.

Geometrical parameters	Values (m)
Turbine diameter (D)	0.9054
Turbine radius (R)	0.4527
Bucket diameter (d)	0.25
Bucket thickness (t)	0.002
Overlap length (e)	0.0906
Overlap ratio (e/D)	0.1
Rotating domain diameter (D_r)	1.1

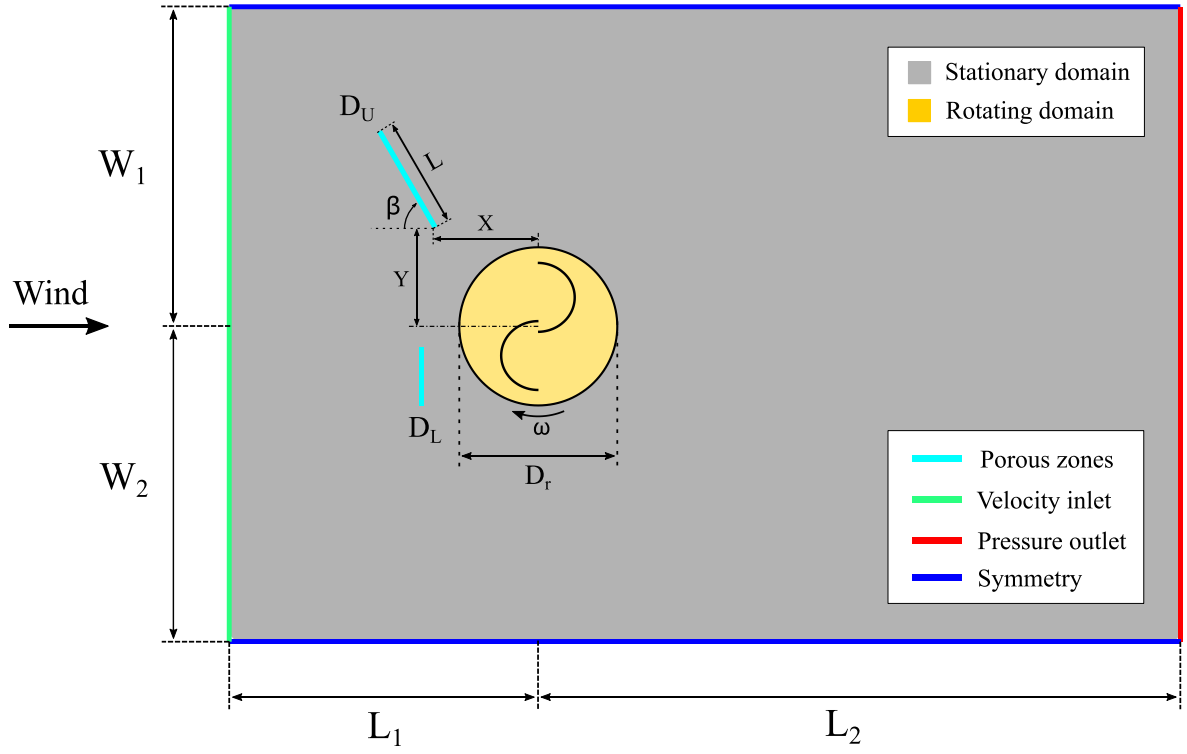

Fig. 2. Computational domain and boundary conditions.

A hybrid mesh containing structured quadrilateral and unstructured triangular elements was created on the rotating and stationary domain as illustrated in Fig. 3. The grid is refined at the zones of interest rather than the whole domain to decrease the computational time. A relatively finer mesh was generated in the rotating and porous zones, compared to the stationary zone.

Preprints (www.preprints.org) | NOT PEER-REVIEWED | Posted: 17 August 2022 doi:10.20944/preprints202208.0296.v1

Structured meshing was done exclusively for the porous deflectors as shown in Fig. 3c. Fifteen inflation layers were employed to mesh the buckets of the turbine as depicted in Fig. 3b. The first layer height of the inflation layers was chosen to be 0.08 mm. A growth rate was also used to gradually decrease the number of mesh elements further away from the interfaces and the turbine buckets.

Table 2. Porous deflector parameters and position

Deflector	Parameters	Values/Ranges
Lower deflector (D_L) [34]	Porosity	0.9
	Angle	90°
	Horizontal distance	0.99D
	Deflector height (length)	0.257D
Upper deflector (D_U)	Porosity (ψ)	0.4-0.9
	Angle (β)	60°-120°
	Horizontal distance (X)	0.1-1D
	Vertical distance (Y)	0.6-1D
	Length (L)	0.25-1D

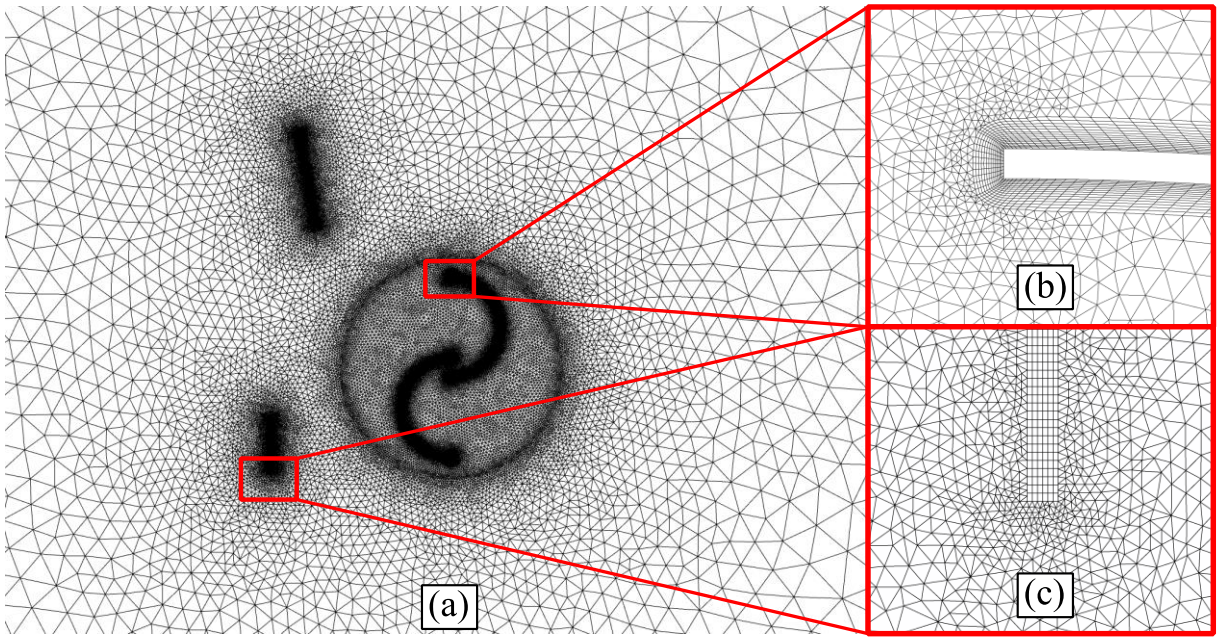

Fig. 3. Generated mesh: (a) Turbine and the deflectors (b) Inflation layers around the turbine blades. (c) Structured mesh in porous deflector zones

Preprints (www.preprints.org) | NOT PEER-REVIEWED | Posted: 17 August 2022 doi:10.20944/preprints202208.0296.v1

3. Methodology

Computational Fluid Dynamics or CFD is an excellent way to simulate experimental studies with minimal use of resources and time. This reduces the expenses and other environmental uncertainties that might be associated with experimental studies and provides an estimation with reasonable accuracy.

3.1. Governing equations

In the present study, an incompressible 2D Unsteady Reynolds-Averaged Navier Stokes (URANS) formulation was utilized to solve the flow field numerically. Fluid flow inside the porous deflectors was modeled by incorporating Darcy and Forchheimer terms into the momentum equation. The governing equations are –

$$\frac{\partial}{\partial x_i}(u_i) = 0 \tag{1}$$

$$\rho\frac{\partial}{\partial t}(u_i) + \rho\frac{\partial}{\partial x_j}(u_i u_j) = -\frac{\partial P}{\partial x_i} + \mu\frac{\partial}{\partial x_j}\left(\frac{\partial u_i}{\partial x_j}\right) + \frac{\partial}{\partial x_j}\left(-\rho\underline{u_j}'\,\underline{u_i}'\right) + S_i \tag{2}$$

Here, the term $-\rho\underline{u_j}'\,\underline{u_i}'$ is the Reynolds stress modeled by the k-ω SST model, u_i is the velocity component, P is pressure, and μ is the dynamic viscosity of the fluid. In equation 2, the source term, S_i applies only for the porous medium, and elsewhere it is zero. S_i is defined as [35] –

$$S_i = -\frac{\mu}{K}u_i - \frac{C_2}{2}\rho|u|u_i \tag{3}$$

Here, K and C_2 are permeability and inertial resistance factors of the porous media respectively. They are the functions of the porosity and the particle diameter of the porous material of the deflectors [35]. Different porosity values changed the values of inertial resistance and permeability accordingly. These values were modeled using the modified Ergun equation [36].

3.2. Performance parameters

One of the most important parameters for any wind turbine is the tip speed ratio (TSR). TSR describes the ratio between free stream velocity to the linear speed of the turbine blade tips. The rotational speed of the rotor is described in terms of the TSR as follows –

$$\lambda = \frac{\omega R}{U_\infty} \tag{4}$$

Here, ω is the angular velocity of the rotor, and R is the radius of the rotor.

Preprints (www.preprints.org) | NOT PEER-REVIEWED | Posted: 17 August 2022 doi:10.20944/preprints202208.0296.v1

The performance of a Savonius turbine is often indicated by the average power coefficient ($C_{p,\,avg}$) and the moment coefficient ($C_{m,\,avg}$). The instantaneous moment coefficient (C_m) was monitored throughout the turbine revolutions. The average moment coefficient ($C_{m,avg}$) is calculated by averaging the instantaneous moment coefficient (C_m) over one turbine revolution. Instantaneous C_m and C_p are defined as follows –

$$C_m = \frac{T}{\frac{1}{2}\rho A U_\infty^2 R} \tag{5}$$

$$C_p = \frac{P_t}{\frac{1}{2}\rho A U_\infty^3} = \lambda C_m \tag{6}$$

Here, T is effective produced torque, P_t is extracted power, ρ is the air density, U_∞ is the free stream velocity of the air, and A is the projected area swept by the turbine.

3.3. Solver settings and convergence criteria

In this study, the commercial CFD code Ansys Fluent v17 is used to solve the two-dimensional flow field numerically. The k-ω SST turbulence model [37] is used in this study. This model is selected because it comprises the benefits of k-ω model which performs better in viscous sublayer flow along with the advantage of k-ε model which is more suitable in the free streamflow [38]. K-ω SST model toggles between these two models when necessary. The pressure-based coupled solver is used due to its faster convergence than other schemes [39]. The least squares cell-based method was applied for the gradients. The discretization methods were set as power-law scheme for momentum, and second order upwind scheme for all other equations. Power-law scheme was chosen instead of the second order scheme after observing a better fit with the experimental results as explained in section 4.3. Sliding mesh technique was used to achieve the rotational motion of the rotor. A timestep equivalent to 0.5° advance in turbine rotation was selected after the time sensitivity test described in section 4.3. Each time step was iterated 30 times to ensure that the residuals dropped below 10^{-5}. The velocity of the incoming air was 7 m/s, which corresponded to a Reynolds number of 442732.

In this study, the convergence was determined by monitoring the average moment coefficient ($C_{m,avg}$) as the literature suggests. However, unlike most of the literature, the maximum number of revolutions for the turbine was not fixed for every simulation. Doing so would create inconsistency in results, as simulations at different tip speed ratios or any other parameters might require different numbers of turbine revolutions to converge. This phenomenon is well described in Fig. 4, where the convergence behavior of two different simulations is displayed. Thus, all the simulations in the present study were considered to be converged when the variation of $C_{m,avg}$ in two subsequent revolutions became less than 0.05%.

Preprints (www.preprints.org) | NOT PEER-REVIEWED | Posted: 17 August 2022 doi:10.20944/preprints202208.0296.v1

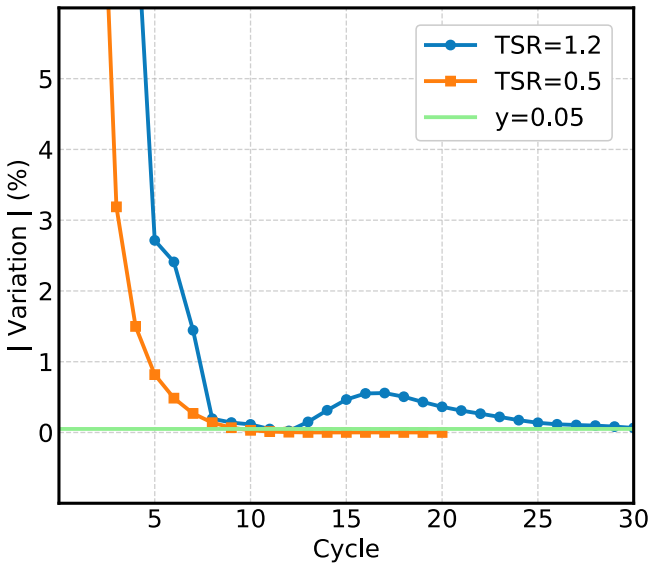

Fig. 4. Convergence behavior for two simulations done at TSR 0.5 and 1.2.

4. Validation

The solution to the numerical simulation must be insensitive to mesh and timestep changes. It is important to get a mesh and timestep independent result while keeping the computational time as low as possible. Additionally, the domain dimensions also play a significant role in determining the solution accuracy. Thus, choosing a balanced mesh and timestep with proper domain dimensions is crucial. Sensitivity tests were performed to find out the suitable mesh, and timestep. Domain dimensions were also investigated.

4.1. Mesh Sensitivity

Normally, with finer meshes, the solution becomes unaffected to further changes in the mesh. The computational time on the other hand greatly increases with the growth in the number of mesh elements. The purpose of the mesh sensitivity test is to find a suitable mesh – one with a lower number of elements that can reproduce the results of the fine mesh. A huge computational time is saved this way, without sacrificing any significant accuracy. In this study, the mesh sensitivity test was performed by monitoring the instantaneous moment coefficient (C_m) throughout one turbine revolution for three different meshes. The meshes were fine, medium, and coarse mesh having 172k, 95k, and 52k cells respectively.

Preprints (www.preprints.org) | NOT PEER-REVIEWED | Posted: 17 August 2022 doi:10.20944/preprints202208.0296.v1

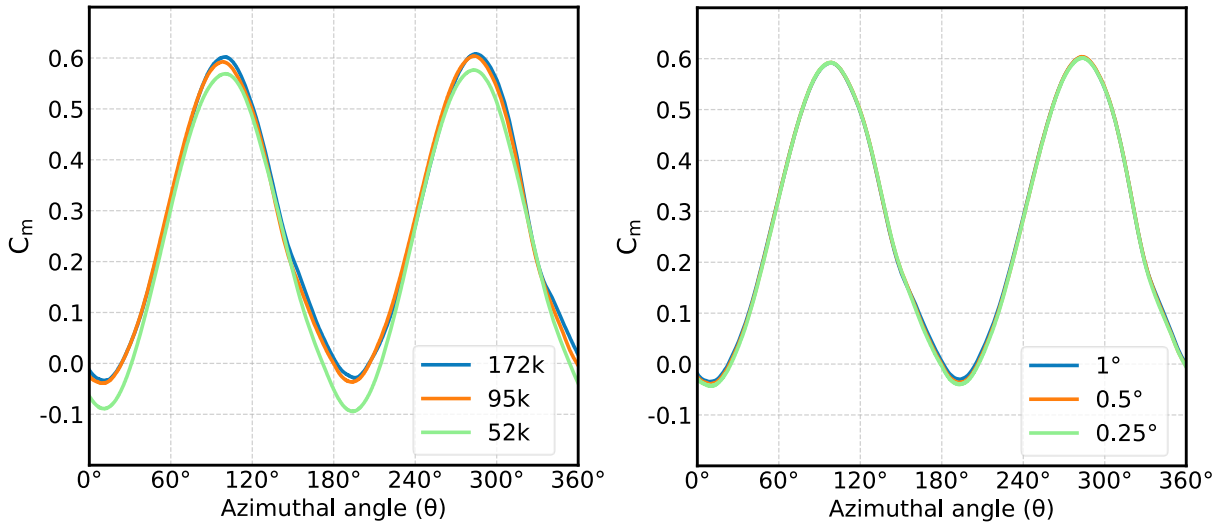

Fig. 5. (a). Mesh sensitivity test at TSR 1 (b). Timestep sensitivity test at TSR 1.

The comparison for the three meshes is shown in Fig. 5a. It is seen that the solution from the medium mesh (95k) is consistent with the fine mesh, i.e., refining the medium does not change the solution. Indeed, the difference between the average moment coefficient ($C_{m,avg}$) for the medium and fine mesh is less than 1%. Thus, further simulations were carried on with the medium mesh (95k).

4.2. Timestep Sensitivity

The timestep sensitivity test helps determine the suitable timestep for performing the simulations. The solution usually gets more accurate with smaller timesteps which, inconveniently, increases the computational time. A relatively bigger timestep is chosen that generates results similar to that of the smaller timestep with minimal variation. Similar to the mesh sensitivity test, three different timesteps were compared to find out the suitable timestep. The timesteps were equivalent to 1°, 0.5°, and 0.25° of turbine revolution.

It is seen from Fig. 5b, there is no significant difference (<1%) between the results with 0.5° and 0.25° timesteps. Consequently, the suitable timestep was chosen to be 0.5°, and further simulations were run with this timestep.

4.3. Validation with experimental study

The numerical method should be validated before proceeding with the simulations. In this study, the experimental study of Sheldahl et. al [8] was selected for validation. Two different schemes for the momentum discretization were used in the simulations – the 2nd order upwind scheme and the power law. All the other discretizations were kept the same as described before in section 3.3. Fig. 6 shows the average power coefficient ($C_{p,avg}$) vs TSR for the experiment and two

Preprints (www.preprints.org) | NOT PEER-REVIEWED | Posted: 17 August 2022 doi:10.20944/preprints202208.0296.v1

aforementioned simulation methods. It is evident that the numerical solution with the Power Law scheme reproduces the experimental results much more consistently, especially after TSR 0.8. Indeed, the power law scheme accurately predicts the peak performance to be at TSR 0.9, while the $C_{m,avg}$ for 2nd order upwind scheme peaks at TSR 1. The 2nd order scheme seems to have a better agreement with the experiment in lower TSRs. However, as the TSR increases, the solution becomes oscillatory with the 2nd order discretization sooner (TSR > 1.2) compared to power law (TSR > 1.4). Thus, the power law scheme was used for the momentum discretization in this study.

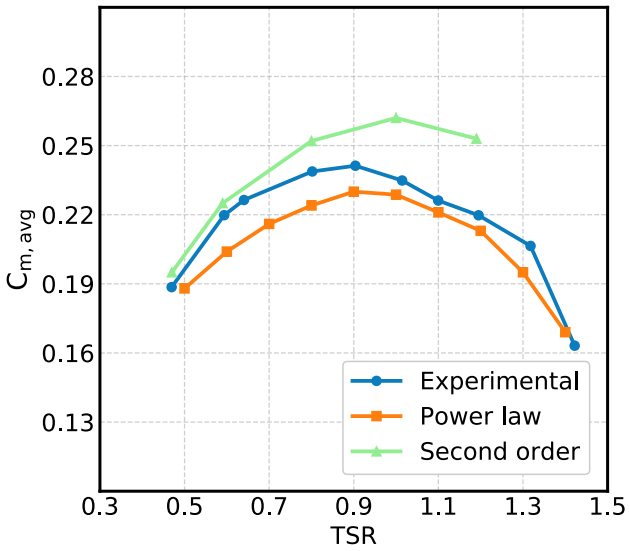

Fig. 6. Validation with experimental study [8] using two momentum discretization schemes.

4.4. Effect of domain size

Domain size plays an important role in the numerical simulation of a wind turbine. Four domains with different dimensions are listed in Table 3. The validation was done with the "A1" domain, following numerous previous studies [13], [34]. However, upon adding the upper porous deflector (D_U), a significant overestimation of the power coefficient may result from using the same domain (A1). This is due to the increased blockage effect introduced by the upper deflector and the symmetry boundary condition, which only allows the flow to be parallel to itself [40]. This effect becomes negligible with a large enough domain. Four sets of domain dimensions (Table 3 and Fig. 7) have been investigated to obtain the optimum domain dimensions. The simulations for domain sensitivity were done at TSR 1.2 with the maximum upper deflector length used in this work, i.e., 1D, with $\beta = 90°$, since this configuration produces maximum blockage. The difference in $C_{m,avg}$ using domain A3 and A4 is ~2% (Fig. 7). Hence, the 3x domain (A3) was chosen for computational efficiency.

Preprints (www.preprints.org) | NOT PEER-REVIEWED | Posted: 17 August 2022 doi:10.20944/preprints202208.0296.v1

Table 3. Domain sensitivity test

Dimensions / Domain name	L1	L2	W1	W2
A1	8D	16D	10D	10D
A2	16D	32D	20D	20D
A3	24D	48D	30D	30D
A4	32D	64D	40D	40D

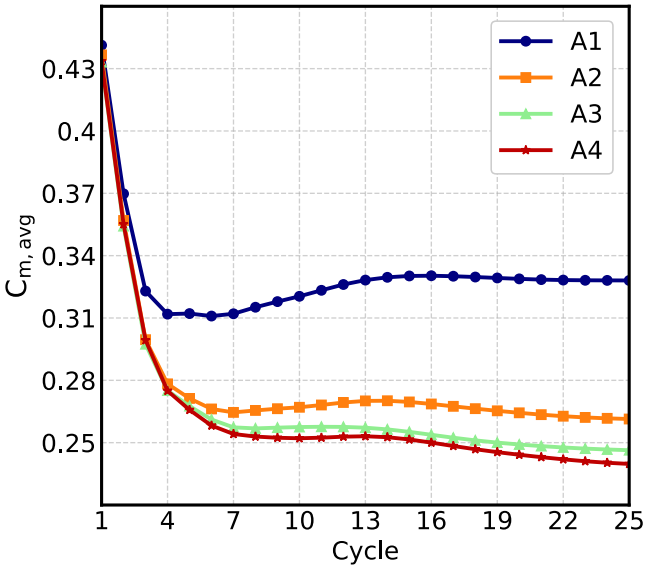

Fig. 7. Comparison of $C_{m,avg}$ calculated using four different domains for the maximum blockage case at TSR 1.2

5. Results and discussions

In this present study, two porous deflectors were placed upstream of the turbine to investigate the combined effect of both porous deflectors on the performance of the Savonius wind turbine. To accomplish this task, one deflector was maintained at the optimum condition as suggested by Nimvari et al. [34], and this deflector was named as 'lower deflector'. The other deflector, placed near the advancing blade, was referred to as the 'upper deflector'. Several parameters of the upper deflector such as porosity, angle, position, and length, were varied sequentially to maximize the turbine efficiency. Afterward, the obtained two deflector configuration was used to assess the overall performance of the turbine and compare it with the previous single porous deflector configuration by [34].

Preprints (www.preprints.org) | NOT PEER-REVIEWED | Posted: 17 August 2022 doi:10.20944/preprints202208.0296.v1

5.1. Optimization of Upper Deflector Parameters

The upper deflector parameters such as deflector porosity (ψ), angle (β), position (X, Y), and length (L) – all play significant roles in determining the efficiency of the turbine. These parameters should be optimized for the most efficient design configuration. In the present study, each parameter is optimized individually, i.e., after a parameter is optimized, the resulting configuration was used for optimizing the next parameter.

5.1.1. Effect of upper deflector porosity (ψ)

The porosity of the deflectors has a significant influence on the performance of the Savonius wind turbine. Nimvari et al. [34] first investigated the effect of porosity of the lower deflector on the wind turbine efficiency, and they reported that the Savonius wind turbine gives an optimum performance at porosity 0.9 of the lower deflector. In this study, to observe the effect of upper deflector porosity (ψ) on the performance of the turbine, four different values of porosity (ψ) of the upper deflector (D_U) were chosen. The simulations were run at six different tip speed ratios (TSR), keeping the porosity and the other parameters for the lower deflector constant at its optimized configuration. The upper deflector porosity (ψ) was varied while keeping the other parameters constant with the initial values of angle $\beta = 60^{\circ}$, horizontal position X = 0.8D, vertical position Y = 0.75D, and length L = 0.5D. It was expected that a certain solidity of deflector would direct the incoming airflow towards the turbine most efficiently. The effect of upper deflector porosity (ψ) on the $C_{m,avg}$ and $C_{p,avg}$ at different TSR is shown in Fig. 8. It can be seen that as the porosity of the upper deflector increased, the average power coefficient ($C_{p,avg}$) started to increase compared to the case with no upper deflector. After reaching a certain porosity value, the average power coefficient ($C_{p,avg}$) started decreasing again.

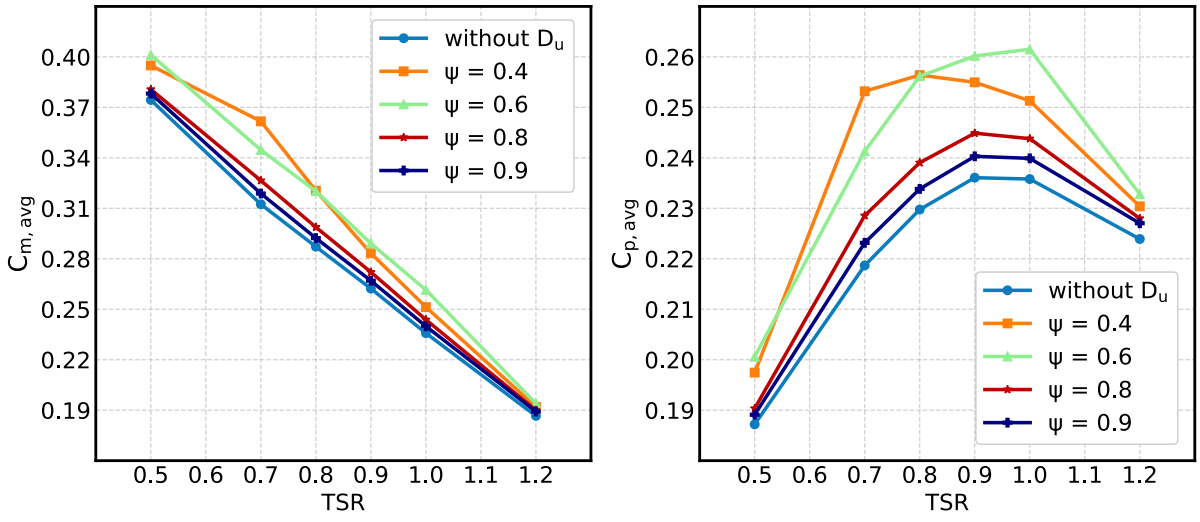

Fig. 8. Effect of upper deflector porosity (ψ) on the average moment ($C_{m,avg}$) and power ($C_{p,avg}$) coefficients.

Preprints (www.preprints.org) | NOT PEER-REVIEWED | Posted: 17 August 2022 doi:10.20944/preprints202208.0296.v1

From the numerical results presented in Fig. 8, it is observed that the maximum power coefficient was achieved at an upper deflector porosity value of 0.6 at almost all of the TSRs considered in this study. The maximum value of the average power coefficient ($C_{p,avg}$) is obtained at TSR 1 with $\psi = 0.6$, which is about 11% higher compared to the case without the upper deflector.

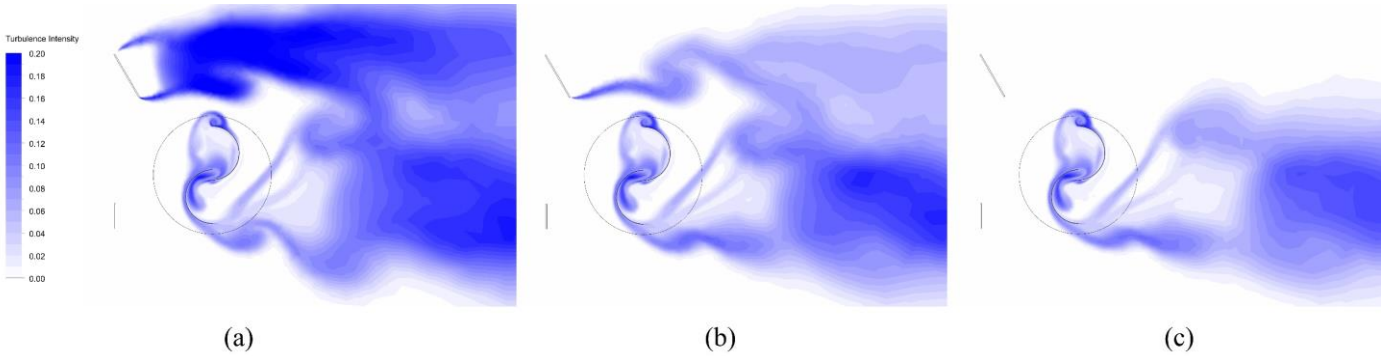

Fig. 9. Comparison between turbulent intensity contours with the upper deflector porosity of (a) 0.4, (b) 0.6, and (c) 0.9 at TSR 1. The porosity of the lower deflector is kept constant at 0.9.

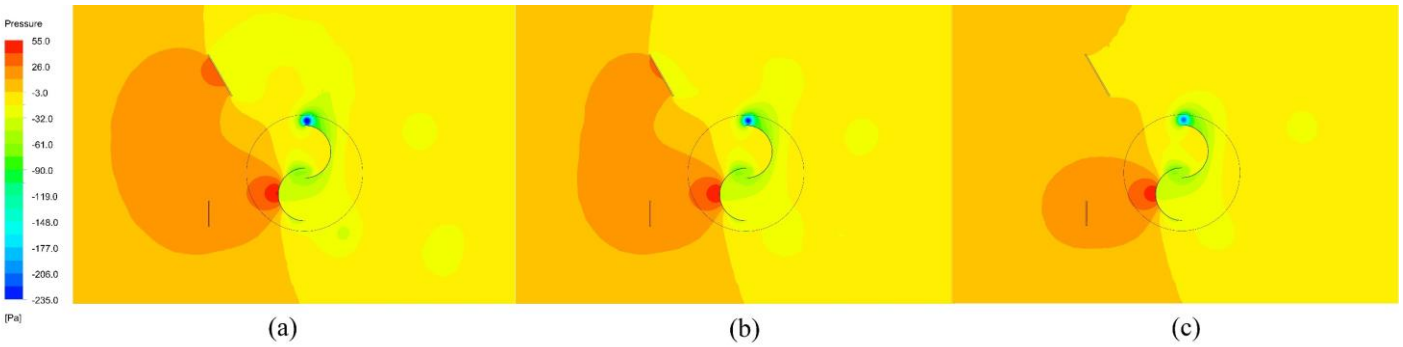

Fig. 10. Comparison between pressure contours with the upper deflector porosity of (a) 0.4, (b) 0.6, and (c) 0.9 at TSR 1. The porosity of the lower deflector is fixed at 0.9.

The effect of porosity on the performance and flow field can be further understood by looking at the turbulent intensity and pressure contour shown respectively in Fig. 9 and 10. From Fig. 9, it is evident that with increasing porosity of the upper deflector (ψ), the region behind the upper deflector and the wake of the turbine becomes less turbulent. In addition, Fig. 10 indicates that as the upper deflector gets less porous, more pressure is created upstream of the turbine. With the value of $\psi = 0.6$, the maximum performance is achieved at TSR 1. This is because the porosity of $\psi = 0.6$ for the upper deflector creates the optimum balance between the turbulence suppression and the positive pressure difference on the advancing blade. The highest porosity of $\psi = 0.9$ causes the lowest turbulence behind the deflector and the wake zone of the turbine. However, it also

Preprints (www.preprints.org) | NOT PEER-REVIEWED | Posted: 17 August 2022 doi:10.20944/preprints202208.0296.v1

creates the lowest pressure difference on the advancing blade of the turbine. On the other hand, the porosity of ψ = 0.4 creates the maximum pressure difference on the advancing blade, but it also adds more turbulent zones and increases the pressure in front of the returning blade as well, causing a lower performance overall.

5.1.2. Effect of the upper deflector angle (β)

The angle of the upper porous deflector (β) was studied with the optimized porosity value (ψ = 0.6). Other parameters were kept at their initial values. The angle was varied from 60° to 120° in an interval of 10 degrees. The effect of the upper deflector angle (β) on the turbine performance is shown in Fig. 11. All the angles of the upper deflector show an improved performance compared to the turbine with only the lower deflector. The performance coefficient started increasing as the angles were increased from 60°. The maximum performance was achieved with β = 80° at TSR 0.9. Both 80° and 100° angles generated very similar performance, however, 80° was chosen due to the maximum $C_{p,avg}$, and better performance in the mid-TSRs.

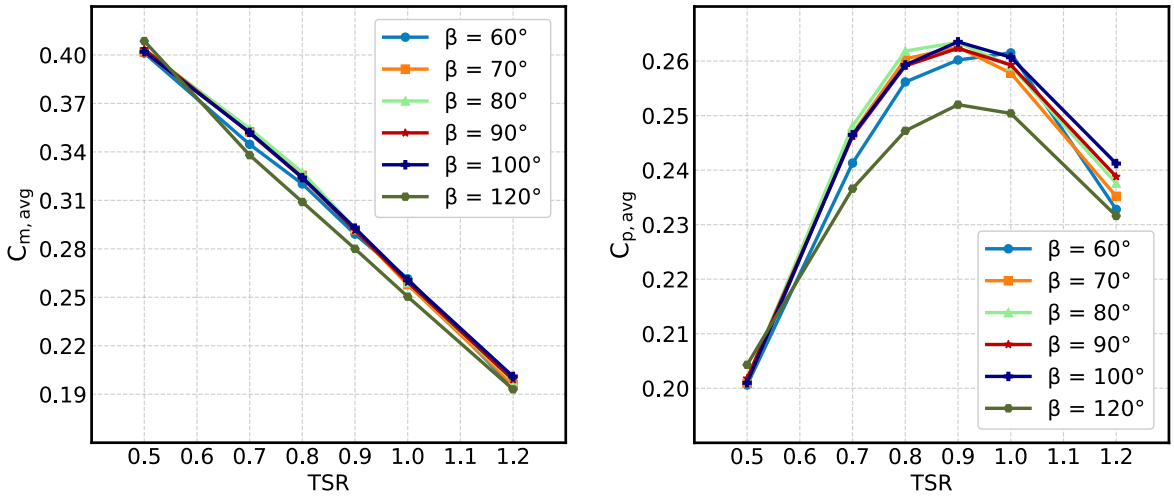

Fig. 11. Effect of upper porous deflector angle (β) on the average moment ($C_{m,avg}$) and power ($C_{p,avg}$) coefficients.

5.1.3. Effect of the upper deflector position (X, Y)

The horizontal distance of the upper deflector from the turbine center (X) was varied to obtain the ideal horizontal position of the deflector. The simulations for X optimization were carried out with the resulting optimized porosity (ψ = 0.6) and angle (β = 80°) of the deflector. The effect of horizontal position (X) on the performance of the turbine is shown in Fig. 12a. It is observed that the performance kept increasing as X decreased until after 0.25D. The performance, however, decreased as the deflector was positioned too close to the turbine (0.1D). Indeed, some of the deflected air passed freely without hitting the advancing blade when the deflector was too close.

Preprints (www.preprints.org) | NOT PEER-REVIEWED | Posted: 17 August 2022 doi:10.20944/preprints202208.0296.v1

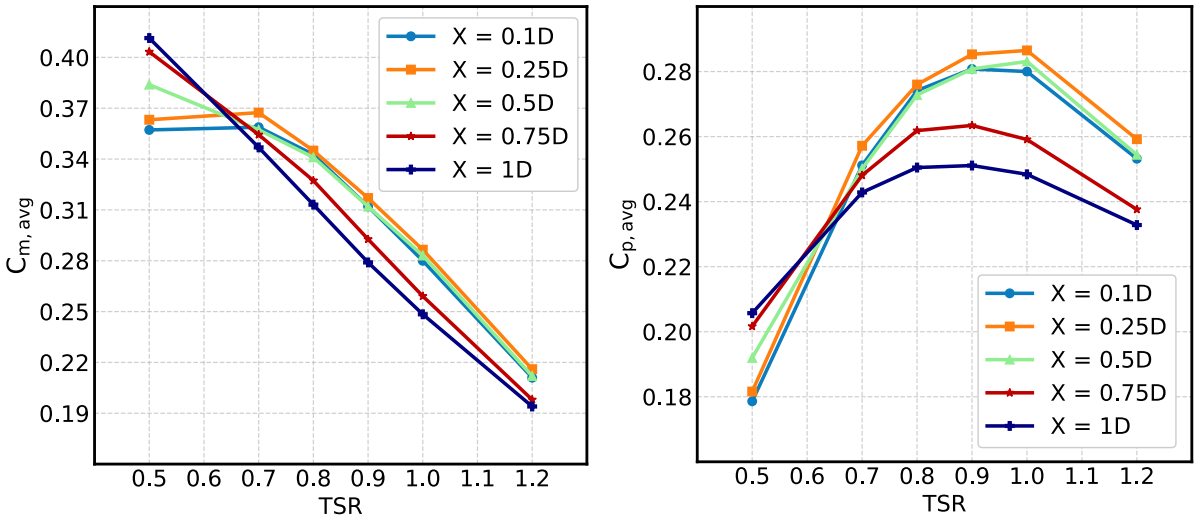

Fig. 12. (a). Effect of upper porous deflector horizontal position (X) on the average moment ($C_{m,avg}$) and power ($C_{p,avg}$) coefficients.

The vertical position of the upper deflector (Y) is an important parameter that considerably affects the performance of the turbine. To investigate this effect, the vertical position was gradually increased from 0.6D to 1D, while keeping the optimized porosity (ψ = 0.6), angle (β = 80°), and horizontal position (X = 0.25D) constant. The effect of vertical position on the performance is portrayed in Fig. 12b. It was found that the upper deflector placed at the vertical position, Y = 0.7D, generates the maximum performance. It is also observed that increment or decrement of vertical position from Y = 0.7D significantly reduces the turbine performance.

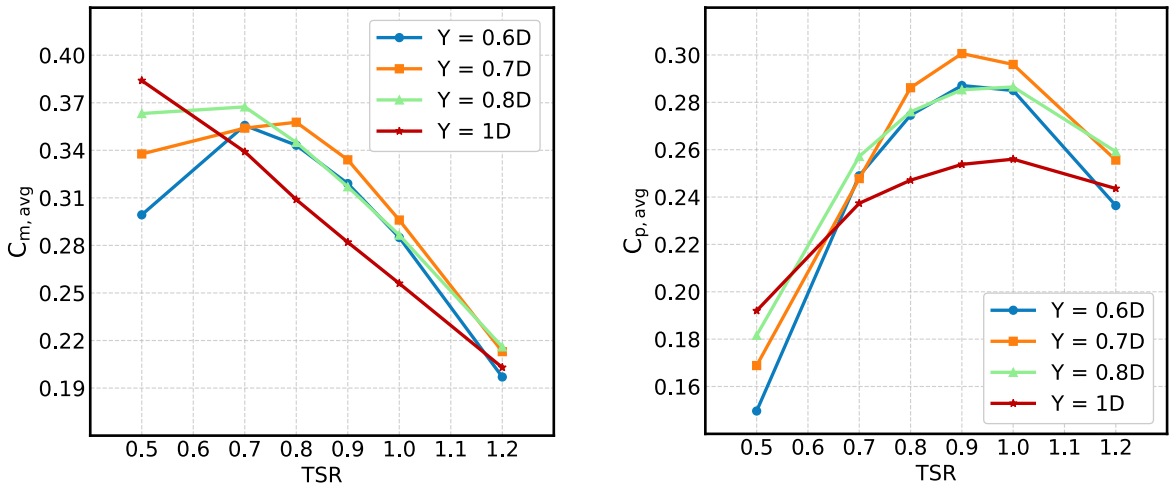

Fig. 12. (b). Effect of upper porous deflector vertical position (Y) on the average moment ($C_{m,avg}$) and power ($C_{p,avg}$) coefficients.

Preprints (www.preprints.org) | NOT PEER-REVIEWED | Posted: 17 August 2022 doi:10.20944/preprints202208.0296.v1

5.1.4. Effect of the upper deflector length (L)

The upper deflector length (L) is another parameter in determining the performance of the turbine. The length was increased from 0.25D to 1D with an interval of 0.25D, keeping all the other parameters in optimized conditions ($\psi = 0.6$, $\beta = 80°$, X = 0.25D, Y = 0.7D). The effect of deflector length on the performance at different TSR is illustrated in Fig. 13. According to Fig. 13, L = 0.5D delivers the best performance for nearly the whole TSR range, and it was chosen as the optimal value for the parameter. The maximum average power coefficient $C_{m,avg}$ was found to be 0.3 at TSR 0.9, a 26% increase compared to the case with only the lower porous deflector.

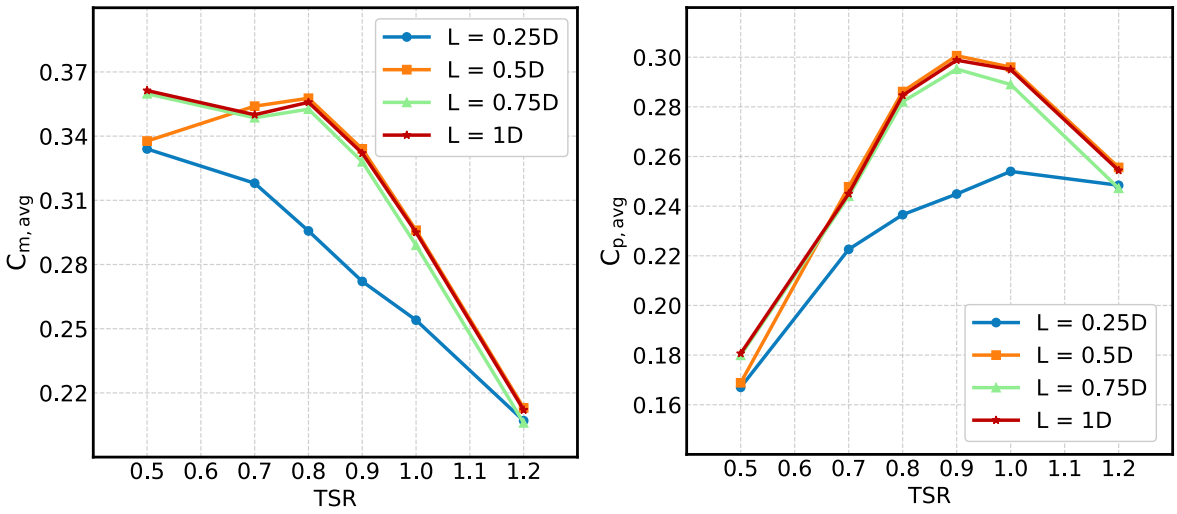

Fig. 13. Effect of upper porous deflector length (L) on the average moment ($C_{m,avg}$) and power ($C_{p,avg}$) coefficients.

5.2. Power and performance analysis

The final configuration of the Savonius turbine needs to be analyzed further to assess the overall performance of the turbine. The average power coefficient ($C_{p,avg}$) is one of the most used indicators of turbine performance. Besides power generation, another important aspect of wind turbines is the self-starting capability at a wide range of tip speed ratios (TSR). The static torque coefficient (C_{ms}) indicates the self-starting performance of a turbine.

5.2.1. Enhancement of average power coefficient

After optimizing the upper porous deflector (D_U), a significant improvement in the power coefficient is observed. The bar chart in Fig. 14 shows the comparison of the average power coefficient ($C_{p,avg}$) at TSR 0.9 among different cases. The case without the upper porous deflector, i.e., only with the lower porous deflector (D_L) improved the power coefficient by about 8.33% compared to the standard Savonius turbine without any deflector. This comparison is done in the

Preprints (www.preprints.org) | NOT PEER-REVIEWED | Posted: 17 August 2022 doi:10.20944/preprints202208.0296.v1

A1 domain. Nimvari et al. [34] found this increase in $C_{p,avg}$ to be 10%, which is in close agreement with the present study.

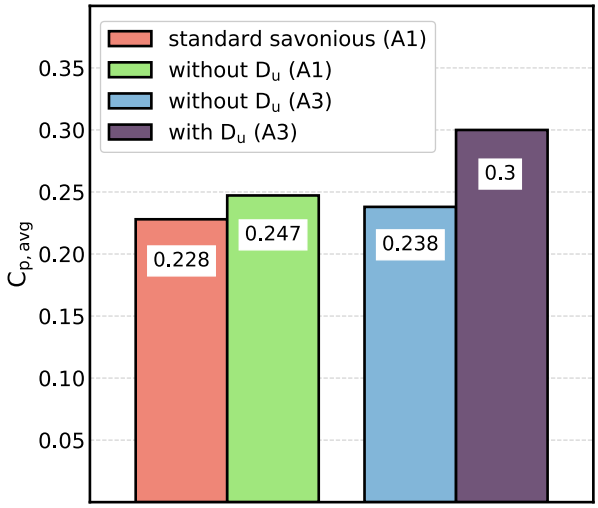

Fig. 14. Comparison between average power coefficient ($C_{p,avg}$) at TSR 0.9 using different cases in different domains.

The present study used a larger A3 domain to minimize the increased blockage effect by the upper deflector (D_U). The case with the optimized upper porous deflector (D_U) increased the $C_{p,avg}$ about 26% compared to the case without upper deflector, both done in the A3 domain.

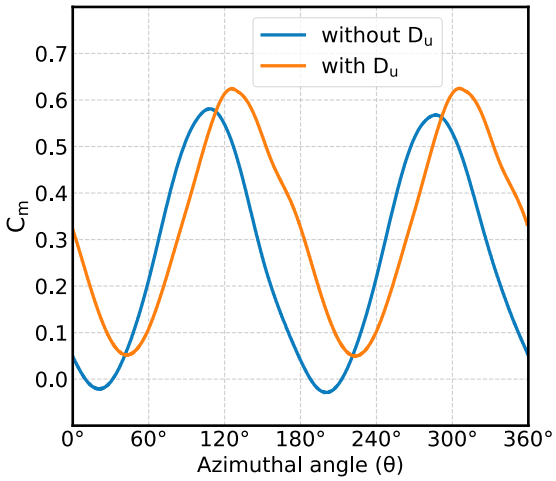

Fig. 15. Comparison in instantaneous C_m between the optimized upper porous deflector (D_U) case and the one without D_U at TSR 0.9, both performed in A3 domain.

The comparison of instantaneous C_m vs θ graph between the no upper deflector case and the optimized upper deflector case is shown in Fig. 15. Negative torque is present for the case with no

Preprints (www.preprints.org) | NOT PEER-REVIEWED | Posted: 17 August 2022 doi:10.20944/preprints202208.0296.v1

upper deflector. In contrast, the optimized upper deflector case has no negative torque throughout the whole turbine revolution. Furthermore, it is observed that a substantial increase in torque is achieved by placing and optimizing the upper porous deflector (D_U). There is an apparent phase difference between the two cases as well. The upper deflector causes the pressure difference on the advancing blade to keep rising later in the revolution compared to the other case. Consequently, the instantaneous moment coefficient (C_m) of the optimized case lags and reaches the peak later.

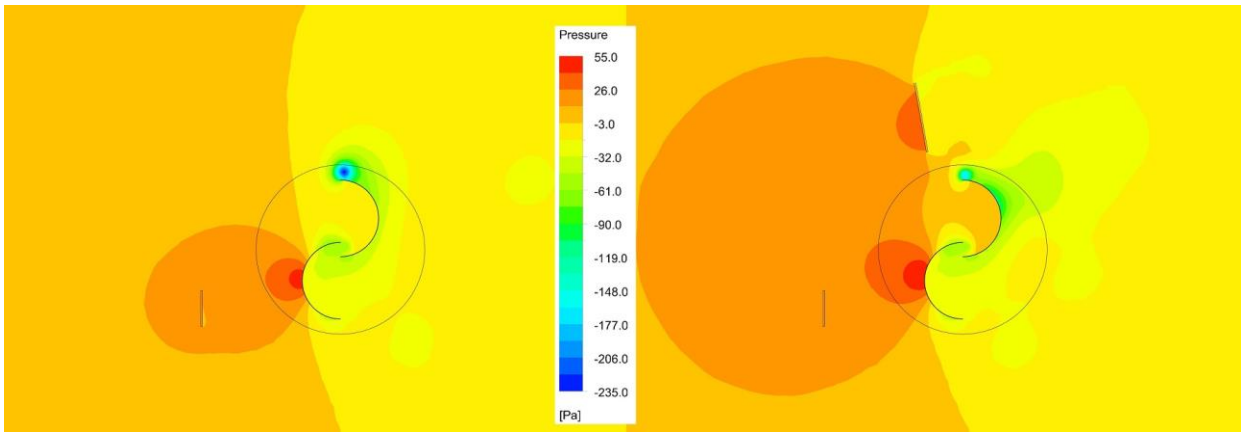

Fig. 16. Pressure contour comparison between the case without upper porous deflector (D_U) and with D_U at TSR 0.9.

The pressure contour for both cases is presented side by side in Fig. 16. It is seen that the upper deflector creates a high-pressure region upwind, thus, the low-pressure vortex on the tip of the blade is reduced. Furthermore, the upper deflector creates a significantly higher pressure difference on the advancing blade compared to the case without D_U.

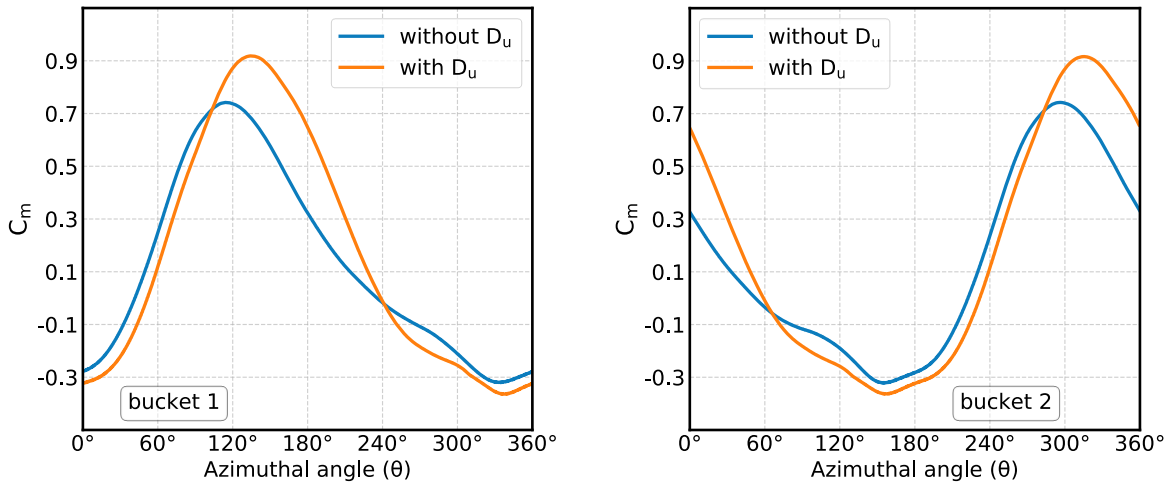

Fig. 17. Instantaneous C_m on individual buckets without upper porous deflector (D_U) and with D_U at TSR 0.9.

Preprints (www.preprints.org) | NOT PEER-REVIEWED | Posted: 17 August 2022 doi:10.20944/preprints202208.0296.v1

The pressure also increases on the returning blade due to the upper deflector, however, the pressure difference on the advancing blade is greater compared to the pressure increase on the returning blade – which ultimately increases the combined instantaneous moment coefficient (C_m). This is also evident in Fig. 17, which shows the torque on individual blades for both cases.

The vorticity contour shown in Fig. 18, only confirms the previously discussed observations. It can be seen that the vortex stream from the lower edge of the upper deflector helps create a low pressure on the convex side of the advancing blade. Additionally, it is also evident that the case with only the lower deflector decreased the pressure on the convex side of the returning blade while the other case increased it slightly due to the influence of the upper porous deflector.

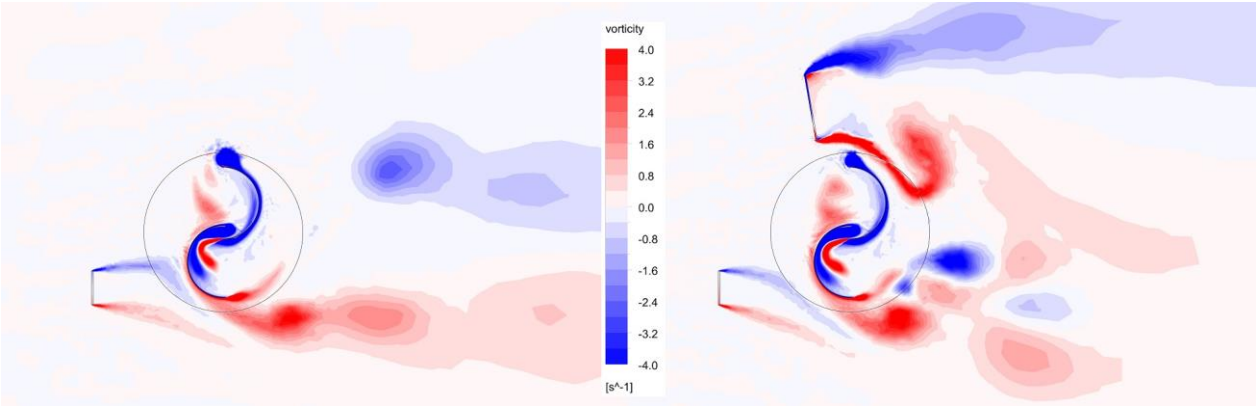

Fig. 18. Vorticity contour comparison between with and without upper porous deflector case at TSR 0.9.

5.2.2. Self-starting performance

The comparison of C_{ms} with and without the upper porous deflector (D_U) is shown in Fig. 19. The figure indicates a period of 180° for the static torque coefficient (C_{ms}). Furthermore, both cases generate a similar C_{ms} profile and positive torque ($C_{ms} > 0$) over the entire azimuthal angle range (0° – 180°), ensuring the self-starting of the turbine. However, the upper deflector increased the static torque coefficient significantly at the azimuthal angle of 80°, where the other case generates very low torque.

Preprints (www.preprints.org) | NOT PEER-REVIEWED | Posted: 17 August 2022 doi:10.20944/preprints202208.0296.v1

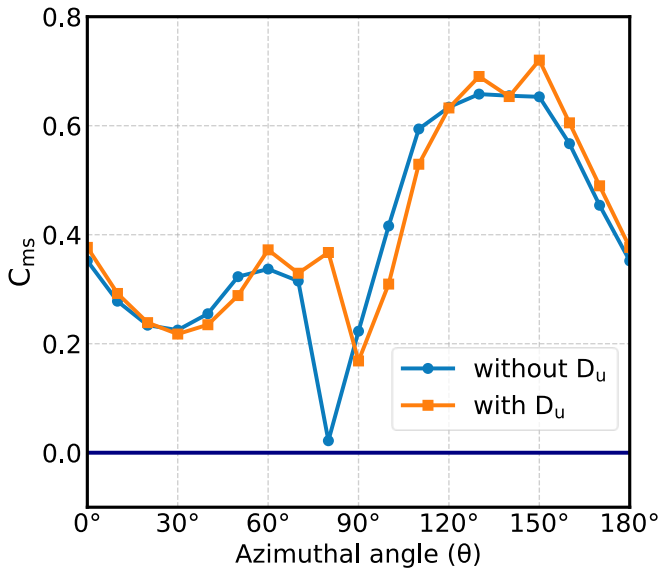

Fig. 19. Static torque coefficient (C_{ms}) with and without upper porous deflector (D_U) done in A3 domain.

6. Conclusion

In this present study, a performance improvement technique for drag-based Savonius turbine has been studied by placing two porous deflectors upstream using a CFD model. The lower porous deflector (D_L) was kept at optimized configurations taken from the work of Nimvari et al. [34]. Several configuration parameters of the upper porous deflector (D_U) such as porosity, angle, position, and length were varied to improve the efficiency of the turbine. The 2D flow field was solved using incompressible unsteady Navier-Stokes equations with the SST k-ω turbulence model. The key finding from this current study is that the placement of the upper porous deflector near the advancing blade improved the performance of the turbine significantly. When the porosity of the upper deflector as well as the angle, position, and length, were optimized, a 26% increase in power co-efficient was found compared to the single porous deflector case reported in current literature. Additionally, the instantaneous C_m vs θ graph with the optimized upper porous deflector case (Fig. 15) produced positive torque throughout the whole turbine revolution. The lowest peak of the graph (Fig. 15) shifted to a higher value as well. The upper deflector created a higher pressure on the concave side of the advancing blade while lowering the pressure on the convex side, thus the pressure difference on the advancing blade increased significantly. The pressure on the returning blade increased as well. However, the pressure difference on the advancing blade was increased much more compared to the returning blade (Fig. 15), which eventually increased the performance of the turbine. The pressure difference on the advancing blade kept rising later in the revolution influenced by the upper deflector, which increased and shifted the peak of the

 doi:10.20944/preprints202208.0296.v1

instantaneous C_m vs θ graph shown in Fig. 15. Furthermore, the domain dimensions played an important role in the numerical simulations, especially with the added blockage effect from the upper porous deflector (D_U). Performing the simulations for the two deflector cases with a smaller domain could have led to an overestimation of the performance coefficients. Thus, the domain dimensions were investigated as well. The static torque coefficients (C_{ms}) using the porous upper deflector were positive in the whole azimuthal angle (θ) range as seen in Fig. 19. The profile was similar to the case without the upper deflector. However, the upper deflector increased the C_{ms} at 80° azimuthal angle, where the other case struggled the most (Fig. 19). In addition, the peak-to-peak difference in instantaneous C_m for the case with two deflectors was also lower (Fig. 15), which could help reduce the fatigue load on the blades of the turbine. While optimizing the upper deflector parameters, the present study did not consider the dependency of the lower deflector, i.e., after introducing the upper deflector, the optimum configuration of the lower deflector might have changed. This could be an excellent direction for future studies.

Acknowledgements

We are immensely grateful to Dr. Mohammad Nasim Hasan for the prudent commentary and early review of our work. We want to thank him for giving us his valuable time to guide us.

References

[1] GWEC (Global Wind Energy Council), “Global Wind Report 2016,” 2017.

[2] S. M. H. Karimian and A. Abdolahifar, “Performance investigation of a new Darrieus Vertical Axis Wind Turbine,” *Energy*, vol. 191, p. 116551, Jan. 2020, doi: 10.1016/j.energy.2019.116551.

[3] M. Al-Ghriybah, M. Fadhli Zulkafli, D. Hissein Didane, and S. Mohd, “The effect of spacing between inner blades on the performance of the Savonius wind turbine,” *Sustain. Energy Technol. Assessments*, vol. 43, p. 100988, Feb. 2021, doi: 10.1016/j.seta.2020.100988.

[4] D. D. D. P. Tjahjana, Z. Arifin, S. Suyitno, W. E. Juwana, A. R. Prabowo, and C. Harsito, “Experimental study of the effect of slotted blades on the Savonius wind turbine performance,” *Theor. Appl. Mech. Lett.*, p. 100249, Apr. 2021, doi: 10.1016/j.taml.2021.100249.

[5] M. Masdari, M. Tahani, M. H. Naderi, and N. Babayan, “Optimization of airfoil Based Savonius wind turbine using coupled discrete vortex method and salp swarm algorithm,” *J. Clean. Prod.*, vol. 222, pp. 47–56, Jun. 2019, doi: 10.1016/j.jclepro.2019.02.237.

[6] K. H. Wong *et al.*, “Experimental and simulation investigation into the effects of a flat plate deflector on vertical axis wind turbine,” *Energy Convers. Manag.*, vol. 160, pp. 109–125, Mar. 2018, doi: 10.1016/j.enconman.2018.01.029.

[7] I. Marinić-Kragić, D. Vučina, and Z. Milas, “Computational analysis of Savonius wind turbine modifications including novel scooplet-based design attained via smart numerical optimization,” *J. Clean. Prod.*, vol. 262, p. 121310, Jul. 2020, doi: 10.1016/j.jclepro.2020.121310.

[8] R. E. Sheldahl, B. F. Blackwell, and L. V. Feltz, “WIND TUNNEL PERFORMANCE DATA

FOR TWO- AND THREE-BUCKET SAVONIUS ROTORS.," *J Energy*, vol. 2, no. 3, 1978, doi: 10.2514/3.47966.

[9] N. H. Mahmoud, A. A. El-Haroun, E. Wahba, and M. H. Nasef, "An experimental study on improvement of Savonius rotor performance," *Alexandria Eng. J.*, vol. 51, no. 1, pp. 19–25, Mar. 2012, doi: 10.1016/j.aej.2012.07.003.

[10] M. A. Kamoji, S. B. Kedare, and S. V. Prabhu, "Experimental investigations on single stage modified Savonius rotor," *Appl. Energy*, vol. 86, no. 7–8, pp. 1064–1073, Jul. 2009, doi: 10.1016/j.apenergy.2008.09.019.

[11] A. Shigetomi, Y. Murai, Y. Tasaka, and Y. Takeda, "Interactive flow field around two Savonius turbines," *Renew. Energy*, vol. 36, no. 2, 2011, doi: 10.1016/j.renene.2010.06.036.

[12] J. H. Lee, Y. T. Lee, and H. C. Lim, "Effect of twist angle on the performance of Savonius wind turbine," *Renew. Energy*, vol. 89, 2016, doi: 10.1016/j.renene.2015.12.012.

[13] W. Tian, Z. Mao, B. Zhang, and Y. Li, "Shape optimization of a Savonius wind rotor with different convex and concave sides," *Renew. Energy*, vol. 117, 2018, doi: 10.1016/j.renene.2017.10.067.

[14] C. M. Chan, H. L. Bai, and D. Q. He, "Blade shape optimization of the Savonius wind turbine using a genetic algorithm," *Appl. Energy*, vol. 213, 2018, doi: 10.1016/j.apenergy.2018.01.029.

[15] N. Alom and U. K. Saha, "Influence of blade profiles on Savonius rotor performance: Numerical simulation and experimental validation," *Energy Convers. Manag.*, vol. 186, pp. 267–277, Apr. 2019, doi: 10.1016/j.enconman.2019.02.058.

[16] M. H. Pranta, M. S. Rabbi, and M. M. Roshid, "A computational study on the aerodynamic performance of modified savonius wind turbine," *Results Eng.*, vol. 10, p. 100237, Jun. 2021, doi: 10.1016/j.rineng.2021.100237.

[17] M. Pourhoseinian, S. Sharifian, and N. Asasian-Kolur, "Unsteady-state numerical analysis of advanced Savonius wind turbine," *Energy Sources, Part A Recover. Util. Environ. Eff.*, 2021, doi: 10.1080/15567036.2020.1859011.

[18] T. Ogawa, H. Yoshida, and Y. Yokota, "Development of rotational speed control systems for a savonius-type wind turbine," *J. Fluids Eng. Trans. ASME*, vol. 111, no. 1, 1989, doi: 10.1115/1.3243598.

[19] W. A. El-Askary, M. H. Nasef, A. A. AbdEL-hamid, and H. E. Gad, "Harvesting wind energy for improving performance of savonius rotor," *J. Wind Eng. Ind. Aerodyn.*, vol. 139, pp. 8–15, Apr. 2015, doi: 10.1016/j.jweia.2015.01.003.

[20] M. Mosbahi, A. Ayadi, Y. Chouaibi, Z. Driss, and T. Tucciarelli, "Performance study of a Helical Savonius hydrokinetic turbine with a new deflector system design," *Energy Convers. Manag.*, vol. 194, pp. 55–74, Aug. 2019, doi: 10.1016/j.enconman.2019.04.080.

[21] Shikha, T. S. Bhatti, and D. P. Kothari, "Vertical axis wind rotor with concentration by convergent nozzles," *Wind Eng.*, vol. 27, no. 6, 2003, doi: 10.1260/030952403773617517.

[22] B. D. Altan, M. Atilgan, and A. Özdamar, "An experimental study on improvement of a Savonius rotor performance with curtaining," *Exp. Therm. Fluid Sci.*, vol. 32, no. 8, 2008, doi: 10.1016/j.expthermflusci.2008.06.006.

[23] S. Sharma and R. K. Sharma, "Performance improvement of Savonius rotor using multiple quarter

blades – A CFD investigation," *Energy Convers. Manag.*, vol. 127, pp. 43–54, Nov. 2016, doi: 10.1016/j.enconman.2016.08.087.

[24] S. Sharma and R. K. Sharma, "CFD investigation to quantify the effect of layered multiple miniature blades on the performance of Savonius rotor," *Energy Convers. Manag.*, vol. 144, pp. 275–285, Jul. 2017, doi: 10.1016/j.enconman.2017.04.059.

[25] B. M. Shaughnessy and S. D. Probert, "Partially-blocked savonius rotor," *Appl. Energy*, vol. 43, no. 4, 1992, doi: 10.1016/0306-2619(92)90024-6.

[26] C. Stout *et al.*, "Efficiency Improvement of Vertical Axis Wind Turbines with an Upstream Deflector," in *Energy Procedia*, Aug. 2017, vol. 118, pp. 141–148, doi: 10.1016/j.egypro.2017.07.032.

[27] K. Golecha, T. I. Eldho, and S. V. Prabhu, "Influence of the deflector plate on the performance of modified Savonius water turbine," *Appl. Energy*, vol. 88, no. 9, 2011, doi: 10.1016/j.apenergy.2011.03.025.

[28] N. P. Putri, T. Yuwono, J. Rustam, P. Purwanto, and G. Bangga, "Experimental studies on the effect of obstacle upstream of a Savonius wind turbine," *SN Appl. Sci.*, vol. 1, no. 10, 2019, doi: 10.1007/s42452-019-1253-2.

[29] F. Guo, B. Song, Z. Mao, and W. Tian, "Experimental and numerical validation of the influence on Savonius turbine caused by rear deflector," *Energy*, vol. 196, p. 117132, Apr. 2020, doi: 10.1016/j.energy.2020.117132.

[30] M. H. Mohamed, G. Janiga, E. Pap, and D. Thèvenin, "Optimization of Savonius turbines using an obstacle shielding the returning blade," *Renew. Energy*, vol. 35, no. 11, pp. 2618–2626, Nov. 2010, doi: 10.1016/j.renene.2010.04.007.

[31] D. Kim and M. Gharib, "Efficiency improvement of straight-bladed vertical-axis wind turbines with an upstream deflector," *J. Wind Eng. Ind. Aerodyn.*, vol. 115, pp. 48–52, Apr. 2013, doi: 10.1016/j.jweia.2013.01.009.

[32] G. Kailash, T. I. Eldho, and S. V. Prabhu, "Performance study of modified savonius water turbine with two deflector plates," *Int. J. Rotating Mach.*, vol. 2012, 2012, doi: 10.1155/2012/679247.

[33] K. M. Youssef, A. M. El Kholy, A. M. Hamed, N. A. Mahmoud, A. M. El Baz, and T. A. Mohamed, "An innovative augmentation technique of savonius wind turbine performance," *Wind Eng.*, vol. 44, no. 1, 2020, doi: 10.1177/0309524X19849860.

[34] M. Eshagh Nimvari, H. Fatahian, and E. Fatahian, "Performance improvement of a Savonius vertical axis wind turbine using a porous deflector," *Energy Convers. Manag.*, vol. 220, 2020, doi: 10.1016/j.enconman.2020.113062.

[35] "Fluent, ANSYS. '14.5-Theory Guide, ANSYS.' Inc., Canonsburg, PA (2012)."

[36] I. F. Macdonald, M. S. El-Sayed, K. Mow, and F. A. L. Dullien, "Flow through Porous Media—the Ergun Equation Revisited," *Ind. Eng. Chem. Fundam.*, vol. 18, no. 3, 1979, doi: 10.1021/i160071a001.

[37] F. R. Menter, "Two-equation eddy-viscosity turbulence models for engineering applications," *AIAA J.*, vol. 32, no. 8, pp. 1598–1605, 1994, doi: 10.2514/3.12149.

[38] K. Y. Chien, "Predictions of channel and boundary-layer flows with a low-reynolds-number turbulence model," *AIAA J.*, vol. 20, no. 1, pp. 33–38, 1982, doi: 10.2514/3.51043.

[39] "M Keating, Accelerating CFD Solutions, https://www.ansys.com/-/media/Ansys/corporate/resourcelibrary/article/AA-V5-I1-Accelerating-CFD-Solutions.pdf."

[40] F. Balduzzi, A. Bianchini, R. Maleci, G. Ferrara, and L. Ferrari, "Critical issues in the CFD simulation of Darrieus wind turbines," *Renew. Energy*, vol. 85, pp. 419–435, Jan. 2016, doi: 10.1016/J.RENENE.2015.06.048.

[41] Islam, A. K. M. S., Islam, M. Q., Razzaque, M. M. and Ashraf, R., "Static Torque and Drag Characteristics of an S-Shaped Savonius Rotor and Prediction of Dynamic Characteristics", Journal of Wind Engineering, Vol. 19, No. 6, U. K., 1995. pp. 363-370.

[42] H. Gad, A. A. El-Hamid, W. El-Askary, M. N.-C. letters, and undefined 2014, "A new design of Savonius wind turbine: numerical study," *researchgate.net*, vol. 6, no. 4, 2014, Accessed: Jul. 06, 2021. [Online]. Available: https://www.researchgate.net/profile/Wa-El-Askary/publication/275990442_A_New_Design_of_Savonius_Wind_Turbine_Numerical_Study/links/554dcc6608ae739bdb8dc633/A-New-Design-of-Savonius-Wind-Turbine-Numerical-Study.pdf.